Materials and Design 85 (2015) 240–247

Contents lists available at ScienceDirect

Materials and Design

journal homepage: www.elsevier.com/locate/jmad

Tailoring a gradient nanostructured age-hardened aluminum alloy using high-gradient strain and strain rate

Pingwei Xu, Hongyun Luo *, Zhiyuan Han, Jian Zou

Key Laboratory of Aerospace Materials and Performance, School of Materials Science and Engineering, Beijing University of Aeronautics and Astronautics, Beijing, People's Republic of China

ARTICLE INFO

Article history:
Received 22 March 2015
Received in revised form 30 June 2015
Accepted 1 July 2015
Available online 6 July 2015

Keywords:
Nanostructured materials
Grain refinement
Strain rate
Strain
Aluminum alloys

ABSTRACT

Microstructural evolution of Al2024 alloy, consisting of precipitates, subjected to surface mechanical grinding treatment (SMGT) was investigated to reveal the role of strain and strain rate in structural refinement. Following SMGT, a gradient nanostructure was formed on the coarse-grained substrate, with a significant increase in nanohardness to over 1 GPa at the top surface. At low strains, the presence of particles and increasing strain rate stimulated the rapid transformation of dislocation configurations. However, at larger strains, increasing strain rate effectively stabilized the fine nanoscale structure. Strain gradient from the deformed layers and near the particles significantly promoted the development of microstructure by increasing the boundary misorientations, which was more significant at high strain rates. In particular, at very high rates and large strain gradients, extreme grain sizes may be induced. The presence of minority grains with size below 10 nm in the top 20-μm layers revealed that dislocation processes still operated at sub-nanoscale level. The dislocation-governed ductility was expected to be improved in the nanostructured materials.

1. Introduction

The drastic refinement in microstructures to submicro- or nanoscale grains, processed by severe plastic deformation (SPD) processes, brings about extraordinary properties in metals and alloys [1–5]. However, it is still challenging to produce nanograins or nanostructures by conventional SPD processes, such as high pressure torsion (HPT) [2–4] and equal channel angular pressing (ECAP) [5–7], in particular, in pure metals due to the limited strain rate ($<1\ s^{-1}$). At room temperature (RT), for instance, pure aluminum (Al) is only reduced to ~800 nm by HPT [8]; however, nanograins are successfully fabricated in pure iron (Fe) [9], copper (Cu) [10,11], nickel (Ni) [12], and titanium (Ti) [13] by surface processes with high strain rate (10^3–$10^5\ s^{-1}$). Among these processes, surface mechanical grinding treatment (SMGT) realizes a thicker hardened layer from the nanostructured surface to the coarse-grained matrix. The gradient microstructure exhibits an excellent combination of properties under tensile load [14–16]. It is convenient to examine the entire process of microstructural evolution down to the nanoscale level attributed to the continuous increase in strain and strain rate with a reducing thickness from surface.

Microstructural refinement is dominated by dislocation motions during deformation, along with the occurrence of twinning [11,17]. During dislocation-induced refinement process, with an increase in the strain, dislocation tangles (DTs) and dense dislocation walls (DDWs) divide the parent grain into dislocation cells (DCs). Subsequently, the low-angle boundary of the cells gradually develops into a high-angle one [9,18]. The cell size d_{DC} is dependent upon the dislocation density and a rough relationship is given by [19]:

$$d_{DC} = K\rho^{-1/2} \tag{1}$$

where K is a constant and ρ is the total dislocation density, which is related to the strain ε. In Lithium fluoride crystals [20], for example, $\rho = 10^9\varepsilon$ when $10^{-3} < \varepsilon < 10^{-1}$. Moreover, the strain rate $\dot{\varepsilon}$ also describes the substructure evolution by utilizing the equation of dislocation dynamics [21]:

$$\dot{\varepsilon} = \alpha b \rho_m v \tag{2}$$

where α is a factor corresponding to ~0.5, b is the magnitude of the Burgers vector, ρ_m is the mobile dislocation density, and v is the average dislocation velocity. Enhanced strain rate effectively suppresses the dynamic recovery because the generated dislocations interact with each other to form various dislocation configurations [22]. Besides, enhanced strain rate increases the dislocation density according to Eq. (2), which leads to a finer grain size as indicated by Eq. (1). Interestingly, increasing strain rate in Cu can change the refinement mechanism [11,23]. Therefore, both strain and strain rate significantly impact the refinement process; however, their individual effect on the microstructural development is not well understood. The theoretically limited grain size (cell size), ~100 nm [11], is larger than the experimental values

* Corresponding author at: 8th Lab of the School of Material Science and Engineering, Beijing University of Aeronautics and Astronautics, No. 37 Xueyuan Road, Haidian District, Beijing 100191, People's Republic of China.
E-mail address: luo7128@163.com (H. Luo).

http://dx.doi.org/10.1016/j.matdes.2015.07.009
0264-1275/

obtained by surface processes [9,23,24]; however, smaller than those by ECAP and HPT [8,25]. The reason for this has not been well understood yet. Besides, the experimental size limit confirms that dislocation mechanism is still operational at this scale. This provides a theoretical guideline for enhancing the dislocation-based properties of the nanostructured metals.

The refinement mechanisms have so far been discussed for single-phase materials or pure metals which have limited their structural use. In contrast to single-phase materials, it is easier to obtain nanostructures in dual- or multi-phase alloys. In cold-drawn pearlitic steel, for instance, ferrite of 18 nm and cementite of 2 nm were obtained with a strain of 3.7 [26]. In a TC 17 alloy with micrometer-sized α-phase embedded into the matrix, mean grain size of 6.7 nm was obtained by air blast shot peening [27]. Therefore, the second-phase particles contribute to microstructural refinement [28–30], depending on their shapes, sizes, distributions, and volume fractions. Moreover, the second-phase particles or precipitates retard recrystallization during deformation at elevated temperature [28], promote dislocation multiplication during early deformation [29,31,32], and increase misorientation between substructures around the particles [30,33]. These examples indicate that the second-phase particle plays a positive role in the formation of a refined microstructure. Although this refinement phenomenon has been comprehensively examined at low strains and strain rates (such as in ECAP and HPT), it is still not well understood at high strain or strain-rate conditions.

The main objective of this study was to reveal the effect of underlying dislocation behavior on structural refinement by simultaneously evaluating the factors such as strain, strain rate, and particles in Al alloys. Al2024 alloy was selected for this study because its refinement process is mainly accommodated by dislocation activities during deformation. This material represents a type of age-hardenable alloys with high specific strength, good fracture toughness, and excellent fatigue properties, whose refinement mechanism may be applicable to many other dual- and multi-phase metals and alloys. It also offers a routine to tailor nanostructured materials having high performance. Moreover, this study provides a new perspective to the understanding of the processes based on dislocation, for e.g. plasticity, at the nanoscale.

2. Experimental

Commercial Al2024 bar with a composition of Al–4.3Cu–1.5Mg–0.6Mn–0.5Fe–0.5Si–0.3Zn–0.1Cr–0.02Ti (wt. %) was used in this study. The bar was machined to 46 mm in diameter and subsequently processed by SMGT with a polycrystalline diamond (PCD) tool at RT, as shown in Fig. 1a. The sample was allowed to rapidly rotate around the z-axis at a speed of N; however, the cylindrical PCD tool (radius: $r = 1$ mm) was slowly slid along the positive z-axis at a speed of f. Penetration of the PCD tip into the sample at an appropriate preset depth a_p resulted in the formation of the plastic deformation zone under the tip, as shown in Fig. 1b. SMGT is a chipless processing; therefore, a fraction of material was pushed in front of the tip and subsequently compressed downwards by the tip. Therefore, this fraction of material suffered a large deformation. The parameters in this study were set as follows: $N = 3000$ rev/min, $f = 5$ μm/rev, and $a_p = 60$ μm.

Following SMGT, the microstructure of the surface layer was investigated and characterized by optical microscopy (OM), transmission electron microscopy (TEM), electron backscatter diffraction microscopy (EBSD), and X-ray diffraction (XRD). Keller's reagent was used to reveal the cross-sectional microstructures. Planar-view foils for the TEM observation at depths were electropolished, in a 25% nitric acid solution in methanol at 245 K and 12 V, only from the bulk side because a plastic film was applied on the other side to prevent any thinning [34]. Prior to electropolishing, layers of various thicknesses were removed from the surface side. Structural sizes below various depths were obtained by measuring two orthogonal axes of the bright areas in dark-field images for 140–650 (sub)-grains. Their means were also recorded. EBSD sample was mechanically polished and then electropolished in a 30% nitric acid solution in methanol at 245 K and 15 V to obtain the fresh surface. The XRD patterns were obtained using a Rigaku D/max2500PC diffractometer with Cu Kα radiation at 40 kV and 200 mA. Scanning speeds of 6 and 0.6°/min were used, respectively, for the conventional analysis and careful observation of peak broadening. Nanoindentation testing was performed on the surface by using an MTS Nano-Indenter XP system with a depth of 1 μm at an indentation strain rate of 0.05 s^{-1} and the sample was prepared similar to the EBSD sample. Surface roughness was measured on the WYKO, model PSL. Experiments related to both the nanohardness and surface roughness were repeated 5 times to obtain the reliable data.

3. Results

3.1. OM microstructure and nanohardness profile

Cross-sectional views of the samples before and after SMGT are presented in Fig. 2a. Inhomogeneous deformation is found at different depths beneath the treated surface due to the difference in grain orientations and structures in the grain interior and grain boundary (GB). The deformed layer is estimated to be ~75 μm in thickness; however, the original grains are ~5–10 μm in size. Furthermore, treated samples exhibit better surface roughness (Ra ≈ 0.14 μm) than the untreated samples (Ra ≈ 0.28 μm). Nanohardness profile as a function of the depth below the surface is shown in Fig. 2b. As the distance from the surface increases, the nanohardness rapidly decreases from 2.89 to 1.81 GPa, and then gradually tends to become steady at the value corresponding to the hardness of the untreated surface. Thus, SMGT leads to a significant increase in hardness over 1 GPa at the topmost surface, as shown in Fig. 2b. The dependence of nanohardness on depth is due to the microstructural variations associated with those depths. Therefore,

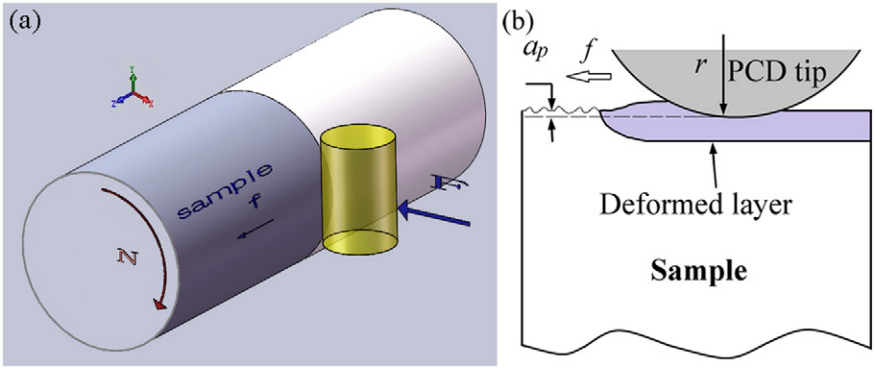

Fig. 1. SMGT processing: (a) schematic illustrations; (b) the plastic deformation layer in Y–Z axis direction.